Excerpt from the Proceedings of the 2011 COMSOL Conference in Boston

Magnetic Nanoparticles for Novel Granular Spintronic Devices - the gGMR sensor

A. Regtmeier*, A. Weddemann**, I. Ennen***, and A. Hütten*

* Bielefeld University, Depart. of Physics, Bielefeld, Germany, anna.regtmeier@physik.uni-bielefeld.de
** Massachusetts Institute of Technology, RLE, MA, USA, weddeman@mit.edu
*** Vienna University of Technology, Institute of Solid State Physics, Vienna, Austria

ABSTRACT

Superparamagnetic nanoparticles have a wide range of applications in modern electric devices. Recent developments have identified them as components for a new type of magnetoresistance sensor based on highly ordered monolayers of such nanocrystallites. In this work, we propose a model for the numeric evaluation of the sensor properties. Based on the solutions of the Landau-Lifshitz-Gilbert equation for a set of homogeneously magnetized spheres arranged in highly symmetric monolayers, we analyze how different device properties may be adjusted to specific demands by modifications of the microstructure. We characterize sensor properties and identify different measurement regimes which correspond to specific dominating energy contributions. In particular, we find a novel measuring mode where increased field sensitivity is bought at the cost of an inherent device noise.

Keywords: magnetic nanoparticles, monolayers, granular giant magnetoresistance, magnetoresistive sensor

1 INTRODUCTION

Small magnetic nanoparticles have been thoroughly studied during the past decades and, nowadays, form substantial components in a wide range of different applications in the field of MEMS- and NEMS-devices. Due to their permanent magnetic moments, they may be manipulated by inhomogeneous magnetic fields in microfluidic devices which also allows for the selective treatment of malignant cells in human health care by hyperthermia or drug delivery techniques [1].

In static assemblies, *magnetoresistive effects* can be found. As shown in Figure 1(a), the electric resistance of a magnetic particle measured in respect to a reference electrode depends on the relative orientation of the magnetization of the two components. These types of nanostructured devices are called *spintronic*-devices since the electronic properties are affected by a quantum mechanic spin-spin-interaction. We will not go into the details here, but only note that a high scattering of conducting eletrions is obtained for antiparallel alignment while a parallel orientation results in a low electric resistance.

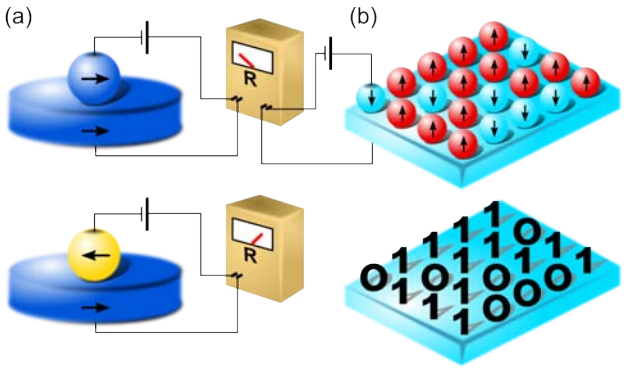

Figure 1: Schematic image of a magnetoresistive device based on magnetic nanoparticles. (a) Resistance of an array of particles and reference electrode. Parallel alignment leads to a lower electric resistance than the antiparallel configuration. (b) A hypothetical array of such particles. Each particle resembles a bit of information where the bit state is defined by the electric resistance value.

If the magnetic moments of individual particles assembled in a particle monolayer would either point down- or upwards, different resistance values could be interpreted by the respective bit-states `0` or `1`, Figure 1(b). Therefore, such an assembly forms a magnetic data storage device with each individual particle resembling one bit of information. Theoretically, data densities of up to 10,000 Gigabit/in^2 could be obtained by this method which is well above densities of modern hard drives (Seagate, up to 625 Gigabit/in^2, 2011). However, hard drive technology is only one of a large variety of applications where such spintronic components play a key role and open up possibilities for novel MEMS- and NEMS-designs.

A new idea based on a similar principle such as the design of granular hard drive technology is the employment of such granular films for the development of a novel type of magnetic field sensor [2]. Commonly, magnetic fields may not be measured directly, but field information is drawn from its perturbation of an undisturbed system. In macroscopic devices, field measurements via the hall effect or induction coils are a standard

procedure. However, in regard to MEMS- and NEMS-technologies where trends tend to increasingly smaller size scales, especially, the electric contacting procedure becomes a crucial factor in the manufacturing process. Also, it may not seem suprising that at these scales different physical phenomena are predominant. Similarly, as for example the dynamics of colloids in liquids are increasingly governed by van der Waals interactions on the nanoscale, in nanoparticalur systems, interatomic coupling effects gain significant importance and may overcome electromagnetic interactions.

In this regard, it is beneficial that various preparation methods are known to obtain highly ordered two-dimensional arrays of magnetic particle films on the micro- or nanoscale [3]. However, with nanoscaled systems significantly less accessible to direct observations, the design of novel devices relies strongly on results of numerical calculations.

2 GOVERNING EQUATIONS

In order to ensure the reliability of the numerical predictions, a strong understanding of the dominant physical properties is important. Therefore, our first step is to develop an accurate framework to calculate the magnetic state of an assembly of magnetic nanoparticles. Along the volume of each particle, a magnetization distribution $\mathbf{M}$ can be found which creates a magnetic stray field in the surrounding space and, in particular, at the positions of nearby particles. From Maxwell's equations of magnetostatic

$$\nabla \cdot \mathbf{B} = 0, \tag{1}$$

$$\nabla \times \mathbf{H} = \mathbf{0}, \tag{2}$$

together with the constitutive law

$$\mathbf{B} = \mu_0(\mathbf{H} + \mathbf{M}), \tag{3}$$

we can calculate the magnetic field $\mathbf{H}$ for a given magnetization distribution $\mathbf{M}$. However, while these equations obviously form a part of our system, they do not provide us with the information we are actually interested in, which is the equilibrium configuration of $\mathbf{M}$ itself.

2.1 Ferromagnetic materials

The dynamic evolution of a magnetization distribution is governed by the phenomenological *Landau-Lifshitz-Gilbert* equation [4]

$$\frac{\partial \mathbf{M}}{\partial t} = -\gamma \mathbf{M} \times \mathbf{H}_{\text{eff}} + \frac{\alpha}{M_{\text{S}}} \mathbf{M} \times \frac{\partial \mathbf{M}}{\partial t}, \tag{4}$$

with M_{S} the *saturation magnetization* which is a material parameter, α a dimensionless damping constant and

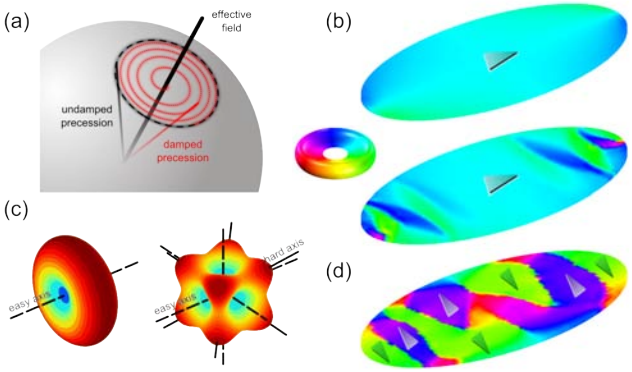

Figure 2: Properties of ferromagnetic systems. (a) Precession of a magnetic moment vector under the influence of an effective magnetic field $\mathbf{H}_{\text{eff}}$ which coincides with the precession axis. The black and red line show undamped and damped precession, $\alpha = 0$ and $\alpha > 0$, respectively. (b) Magnetic distribution in a elliptic thin film for high and low exchange constant. (c) Different anisotropy energy surfaces. The left plot shows an uniaxial symmetry, the right a cubic anisotropy. Red areas coincide with magnetically hard axes, blue with easy axes. (d) Magnetic distribution for uniaxial anisotropy.

γ the gyromagnetic ratio. The two different contributions on the right hand side can be easily visualized as shown in Figure 2(a). The first summand corresponds to a precession term; the magnetization vector $\mathbf{M}$ rotates around an effective magnetic field $\mathbf{H}_{\text{eff}}$. Without the second term, the altitude angle would be a constant of the motion since no energy leaves the system. However, due to local damping mechanisms summarized in the second term, the magnetic vector $\mathbf{M}$ reaches in equilibrium state by alignment with the effective magnetic field vector.

In order to completly specify equation (4), we need to find an appropriate expression for the effective magnetic field $\mathbf{H}_{\text{eff}}$. If we set $\mathbf{M} = M_{\text{S}}\hat{\mathbf{m}}$, commonly, the following decomposition is chosen

$$\mathbf{H}_{\text{eff}} = \frac{2A}{\mu_0 M_{\text{S}}} \Delta \hat{\mathbf{m}} - \frac{1}{\mu_0 M_{\text{S}}} \frac{\delta f_{\text{ani}}(\hat{\mathbf{m}})}{\delta \hat{\mathbf{m}}} + \mathbf{H}_{\text{d}} + \mathbf{H}_{\text{ex}}. \tag{5}$$

So what do all these terms stand for? The first summand refers to a quantum mechanic force, the *exchange coupling*. From a very intuitive point of view, we may visualize a ferromagnetic material by its capability to locally align its magnetization or, in other words, by its tendency to minimize the curvature ΔM_i in the magnetic distribution. In this regard, the exchange constant A may be understood as a measure for the magnetic stiffness of a ferromagnetic material: the higher the value of A, the less magnetic domains are found within the magnetic volume, Figure 2(b). The second term refers to magnetocrystalline anisotropy. Within a finite element simulation, we usually treat the magnetic volume

as a homogeneous, isotropic continuum which is not the case for real systems. The crystallographic (anisotropic) microstructure introduces so called *hard* and *easy directions* which are energetically least and most favorable, respectively. This angular dependency is given by the anisotropy functional f_{ani}, examples are shown in Figure 2(c). The *demagnetization field* $\mathbf{H}_{\text{d}}$ is the magnetic field which results from the magnetic object itself. Commonly, the resulting energy contribution is very low if the total magnetic moment of the considered object is close to 0. Finally, all external field effects are summarized in $\mathbf{H}_{\text{ex}}$.

As stated above, the exchange contribution imposes a strong energy penality along regions where a high curvature in the magnetic distribution can be found. Consequently, high curvature is only present if the energy loss is compensated by the energy gain of another contribution. If we neglect anisotropy effects for the moment, typically, a strong interplay between exchange coupling and stray field energy becomes the main driving force: a highly structured magnetic distribution as shown in Figure 2(b), bottom, minimizes the magnetic stray field energy, but results in a high exchange energy while configuration shown in 2(b), top, entails low exchange but high stray field energy. The influence of a uniaxial anisotropy with easy axis parallel to the short ellipse axis is shown in Figure 2(d). However, the equilibrium state of a system does not only depend on the different material parameters but also on the initial state.

2.2 Magnetic nanoparticles

Equation (4) holds for all types of ferromagnetic systems though, of course, it may not be the most handy form whenever there are additional information on the type of system we are interested in. As stated above, exchange coupling imposes an energy penality along regions with a high curvature in the magnetic distribution. Depending on the value of A, a change of the magnetization direction will only occur on a certain length scale. Therefore, if the dimension of an object in a certain direction $\hat{n}$ falls below this critical size threshold, the change of orientation of magnetic components is very small and may be neglected

$$\langle \hat{n}, \nabla m_i \rangle \approx 0. \tag{6}$$

For magnetic nanoparticles, this holds in *all* directions and we may, therefore, approach their magnetic distributions by a homogeneous magnetization or the particle by magnetic dipole of dipole moment $\mathbf{m}$ which results in the magnetic stray field [5]

$$\mathbf{H}_{\text{dipole}} = \frac{1}{4\mu_0}\left(\frac{\langle \mathbf{r}, \mathbf{m}\rangle \mathbf{r}}{r^5} - \frac{\mathbf{m}}{r^3}\right). \tag{7}$$

By approximating the magnetic state of a nanoparticle by a homogeneous magnetic distribution, the first summand in equation (5) is identical to 0. Consequently,

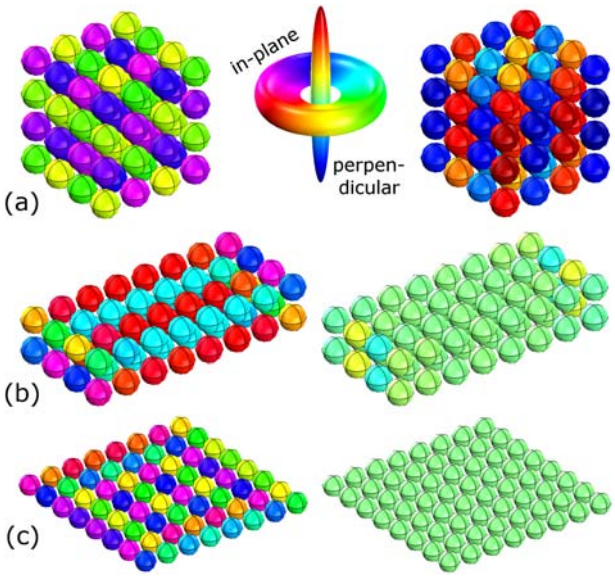

Figure 3: Equilibrium states of various magnetic particle assemblies. Particles with a diameter of $d = 16\,\text{nm}$ and a saturation magnetization of $M_{\text{S}} = 1000\,\text{kA/m}$ are employed. The left side shows the xy-magnetization, the right the z-component.

all partial derivatives in respect to space vanish and instead of solving a set partial differential equations, our model simplifies to a set of ordinary ones. For a set of N such dipole particles, the governing equations may be rewritten in matrix form as [6]

$$(\mathsf{Id} - \alpha \mathsf{M})\frac{\partial \mathsf{m}}{\partial t} = \gamma \mathsf{M}\mathsf{H}_{\text{eff}} \tag{8}$$

with Id the identity mapping on $\mathbb{R}^{3N\times 3N}$, by M the block diagonal matrix

$$\mathsf{M} = \begin{pmatrix} \mathsf{M}_1 & & 0 \\ & \ddots & \\ 0 & & \mathsf{M}_N \end{pmatrix}$$

with $\mathsf{M}_{n,ij} = \epsilon_{ijk}\hat{m}_{n,k}, n = 1, ..., N$ and

$$\frac{\partial \mathsf{m}}{\partial t} = \frac{\partial}{\partial t}(\hat{m}_{x,1}, \hat{m}_{y,1}, ..., \hat{m}_{x,2}, ...)^T$$
$$\mathsf{H}_{\text{eff}} = (H_{\text{eff},x,1}, H_{\text{eff},y,1}, ..., H_{\text{eff},x,2}, ...)^T.$$

These equations were solved in COMSOL Multiphysics employing the micromagnetics plug-in PADIMA. For more information see also [7].

2.3 Equilibrium properties and response functions

In order to obtain a first qualitative understanding of the magnetic behaviour of interacting magnetic monodomain particles, we take a look at the magnetic equilibrium state of different particle assemblies, Figure 3.

The calculations were conducted for 64 particles, arranged in three different cubic assemblies of increasing aspect ratio: (a) $4 \times 4 \times 4$, (b) $8 \times 4 \times 2$ and (c) $8 \times 8 \times 1$. The figure shows azimuthal (colorcode: disc) and out-of-plane (colorcode: cone) magnetic components on the left and right sight, respectively.

In comparison to the continuous ferromagnetic systems (Figure 2), no local ordering can be found in the way that if we choose an arbitrary particle and calculate the magnetic moment of the particle and its neighbors, the resulting value is approximately 0. The absence of exchange coupling due to spatial separation of individual nanoparticles results in a low degree of ordering which minimizes the magnetic stray field energy. Further, by increasing the aspect ratio, (a) $\rightarrow$ (c), the magnetic orientation is increasingly confined into the particle plane. Again, minimization of magnetic field energy is the main driving force. However, it is important to note that modifications of geometrical properties have strong impact on the magnetic state. As we will see later on, this effect may be readily exploited to adjust certain device properties.

If we apply a homogeneous external magnetic field, the response functions show a strong dependency on the field direction. Figure 4 shows the hysteresis loops of the assemblies, i.e., we calculated the magnetic states for different external field values beginning at a magnetic field strength of 100 kA/m which is step-wise reduced to a value of -100 kA/m and afterwards increased again to 100 kA/m. The cubic case $4 \times 4 \times 4$ almost exhibits an isotropic paramagnetic behaviour with only minor hysteresis effects for a field parallel to the [1 1 1]-direction of the cubic lattice (blue line). Contrary, the planar geometry $8 \times 8 \times 1$ shows a strong ferromagnetic characteristic for external fields applied parallel to the particle plane (black, red line) but exhibits a perfect paramagnetic behavior of very low susceptibility for out-of-plane mearsurements (green line).

2.4 Influence of microstructure

In order to design nanoscale devices tailored to specific tasks, we need to understand how various parameters within the setup influence the response properties. So what are the degrees of freedom in our system that can easily be manipulated in regards to the experimental sample preparation? There is a wide range of different approaches that either affect the magnetic nanocomponents or the assembly as a whole. Here are four examples:

assembly symmetry: Different preparation methods of particle assemblies may result in different spatial ordering such as cubic or hexagonal lattice symmetries.

impurities: Impurities may be introduced by various approaches such as employing particles with a wide size distribution or mixing magnetic and non-magnetic nanocrystals.

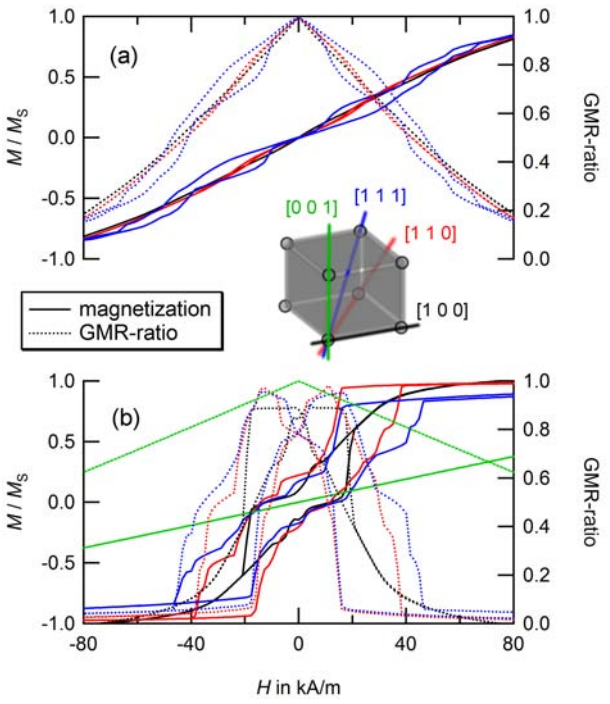

Figure 4: Response of magnetic particle ensembles to an external magnetic field for (a) $4 \times 4 \times 4$ and (b) $8 \times 8 \times 1$ along indicated crystallographic axes.

particle magnetism: Particles of different materials can be employed. Nowadays, there are lots of particle species available commercially.

particle crystallography: Depending on the material history, same materials may be present in different crystallographic phases which introduces different anisotropy scenarios.

In order to get a first impression on how different variations influence the magnetic response properties, we introduce a reference system. This reference system consists of 10×10 particles which are assembled in a hexagonal lattice with lattice constant $a = 20$ nm. The particle radius is set to $R_\mathrm{P} = 8$ nm, the saturation magnetization to $M_\mathrm{P} = 1000$ kA/m and the anisotropy functional to $f_\mathrm{ani} \equiv 0$. For comparison, we only change one of the parameters at a time and leave all remaining ones unchanged:

1. $M_\mathrm{P} = 2000$ kA/m
2. unaxial magnetocrystalline anisotropy
3. cubic magnetocrystalline anisotropy
4. introduce 50 vacancies

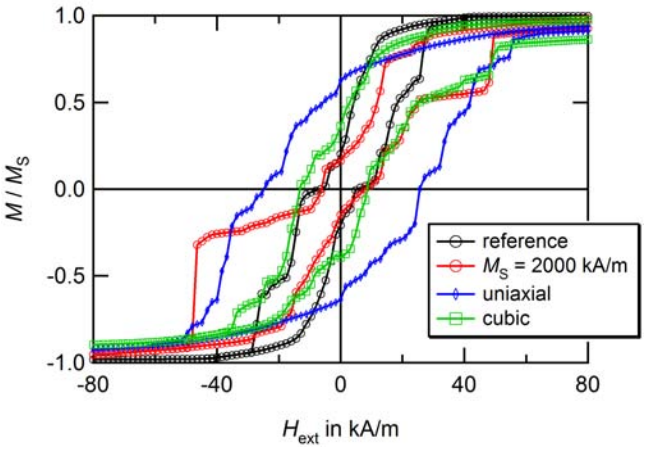

Figure 5: Hysteretic response of arrays of 10×10 magnetic nanoparticles for different particle properties.

Results for the different scenarios 1 to 3 together with the reference sample are shown in Figure 5. A higher magnetic moment (red line) increases the magnetic fields necessary to break the interparticular dipole coupling and, therefore, the sample reaches a saturated state for higher field strengths. Different anisotropy assumptions result in increased coercive and saturating magnetic fields. In general, the more easy axes can be found in a material, the softer the switching behavior which coincides with our results when comparing the uniaxial (blue) to the cubic (green) or isotropic anisotropy case.

The influence of vacancies is shown in Figure 6. Similarly to the influence of uniaxial anisotropy, the resulting response curve shows a much higher coercive field in comparison to the reference system. Indeed, vacancies introduce a local geometric shape anisotropy. As indicated in Figure 6, in the equilibrium state, the magnetic alignment follows the microstructure of the system which introduces an additional energy barrier and, consequently, a harder switching characteristic. We already observed this when increasing the aspect ratio of the 64-particle array, Figure 3 for the out-of-plane component. Here, in contrast to the previous case, each subsystem has two stable configurations given by the two different magnetization directions. However, the energy barrier to switch between these states is very high and, consequently, an increased hysteresis is entailed.

3 TRANSPORT PROPERTIES

From the magnetic properties of an object and its magnetic responses to an external perturbation, many information about the external source may be concluded [8]. Unfortunately though, this would require the real-time measurement of the systems magnetic properties itself. A physical quantity that can measured at a very high precission is voltage or, if the current over the device is

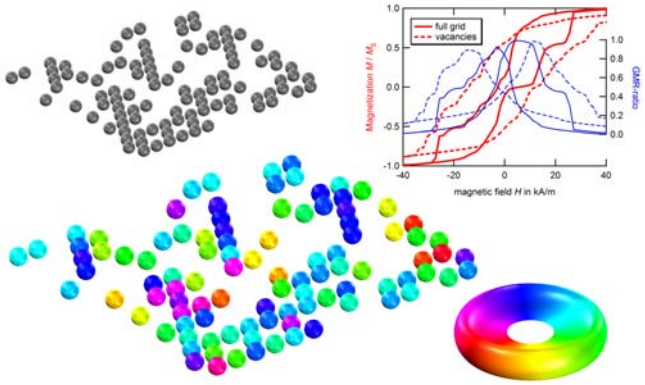

Figure 6: Influence of vacancies: magnetic moments align with the geometric microstructure of the assembly which entails a significant increase of the coercive field due to a high local geometric shape anisotropy.

a constant, resistance. Now, if it would be possible to find a relation between the magnetic properties of the granular film system and the magnetic response, similar to the single particle systems shown in Figure 1, it should be possible to measure a magnetic field by means of measuring the electric response of the device.

3.1 GMR effect in granular systems

The *giant magnetoresistance* (GMR, Noble prize, 2007) effect was originally found and studied in magnetic multilayer systems [9], [10]. The resistance of a magnetic thin film device varies strongly depending on the relative orientation of the magnetization within the layers and, therefore, can be manipulated by an external magnetic field. In 1992, Berkowitz et al. [11] and, independently, Xiao et al. [12] reported similar observations within granular systems of magnetic particles encapsulated in a metallic matrix. The relative increase of resistance, the *GMR-ratio*, of such discrete magnetic patterns is correlated to the deviations of the angular distribution from the average direction. According to V. Wiser [13], it is

$$\mathrm{GMR} = 1 - \frac{C}{2}\langle 1 + \cos\theta \rangle^2, \tag{9}$$

where C is a mearsure for the spin dependence of electron scattering and θ the angle between adjacent magnetic moments. For the sake of simplicity, we will set $C = 1$ in the following.

How does this help to design a nanoscale magnetic field sensor? To understand this, let's just evaluate equation (9) for different limit cases. If we apply a very strong homogeneous magnetic field, the dipolar particle coupling will be overcome and the magnetic moment of each particle aligns with the field direction. Therefore, all moments point into the same (and average) direction and we have $\theta \equiv 0$ and with $C = 1$ also $\mathrm{GMR} = 0$. A

homogeneous magnetic distribution or a strong homogeneous perturbation field result in a low electric resistance. In the opposite case, that there is no magnetic field applied, we have already seen that the ensemble reaches an equilibrium state with a vanishing magnetic moment and a low degree of magnetic order. Consequently, low external fields that do not overcome the dipolar coupling result in a high electric resistance or high GMR-ratio ≈ 1.

For the experimental realization, the particle monolayer needs to be surrounded by a conducting matrix. This can be achieved by depositing a thin metallic film e.g. via a sputtering procedure. At the moment, we will neglect possible influences of this metallic filler in our analyses. However, additional calculations need to be carried out in the near future incorporating possible linear and biquadratic coupling phenomena between contiguous nanocrystals.

3.2 The gGMR-sensor

At this stage, we have basically developed the conceptional basis of a novel type of granular giant magnetoresistance (gGMR) sensor. This type of device offers one major advantage in comparison to continuous magnetic film arrays. When trying to downscale thin magnetic films, they reach a size scale (at about several hundred nanometers) where magnetic exchange coupling becomes the dominating force in the system and makes their magnetic behavior very stiff. Hence, their response to an external perturbation is commonly below the thermal device noise and it is not possible to measure any signal. Via spatial separation of individual magnetic cores, we have overcome exchange coupling. Individual particles are much more free to align their magnetic moment parallel to external fields and, therefore, an increased response to even field of small strengths on the nanoscale is expected.

In order to study the array's capability to detect and measure magnetic fields, we introduce a probe particle that is placed on top of the array in some distance and calculate the response. Again, we assume a 10×10-array of hexagonally ordered isotropic particles of magnetization M_S and radius $R = 8\,\mathrm{nm}$. For the probe particle, we set $R_\mathrm{P} = 20\,\mathrm{nm}$, $M_\mathrm{P} = 1000\,\mathrm{kA/m}$ and place it at a height of $z_0 = 50$ and $100\,\mathrm{nm}$. The corresponding response maps for the particle placed at different (x, y, z_0) coordinates is shown in Figure 7.

If the probe particle is placed at some distance, the resulting GMR-response map (top) shows a very smooth characteristic while the GMR-amplitude, the difference between maximum and minimum value reached, of about 3.6% is not very high which would only allow for low temperature applications. However, we observe a significant increase to about 16% if the probe particle gets closer to the sensor. As we can see, this increased sensitivity is bought at the cost of an inherent device noise.

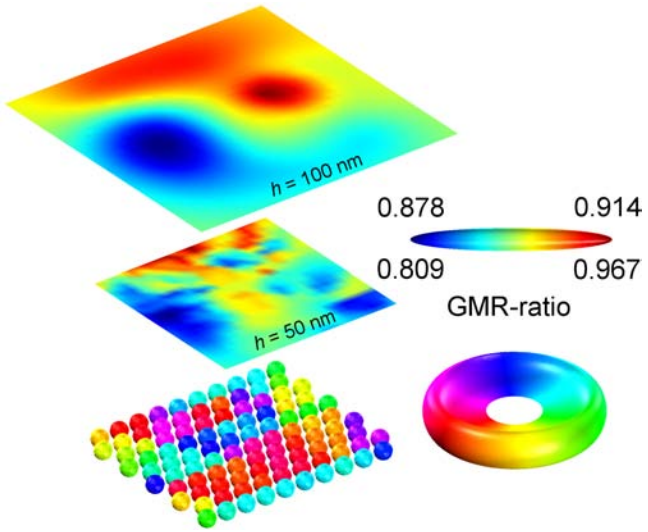

Figure 7: Magnetic response in respect to the position of a probe particle of radius R_P, magnetization $M_\mathrm{P} = 1000\,\mathrm{kA/m}$ at heights $z_0 = 50$ and $100\,\mathrm{nm}$.

CONCLUSION

We have developed a numerical model for the simulation of discrete dipolar magnetic particles and successfully implemented the governing equations into COMSOL Multiphysics. This framework allows for the analysis of properties of magnetic particles arrays such as anisotropic response functions, coercive fields and hysteretic behavior. The modeling led to the conceptional design of a novel type of spintronic devices. First experimental realizations based on the numerical results show the predicted characteristics and features.

Acknowledgements

This work was supported by the FOR 945 and the SFB 613 in the framework of project 3 and project K3, respectively. A. Weddemann gratefully acknowledges the financial support of the Alexander von Humboldt foundation.

REFERENCES

[1] N. Pamme. *Magnetism and microfluidics.* Lab Chip *6*, 24-38, **2006**.

[2] A. Weddemann, I. Ennen, A. Regtmeier, C. Albon, A. Wolff, K. Eckstädt, N. Mill, M.K.H. Peter, J. Mattay, C. Plattner, N. Sewald, A. Hütten. *Review and outlook: from single nanoparticles to self-assembled monolayers and granular GMR sensors.* Beilstein J. Nanotech. *1*, 75-93, **2010**.

[3] A. Weddemann, F. Wittbracht, B. Eickenberg, A. Hütten. *Magnetic Field Induced Assembly of Highly Ordered Two-Dimensional Particle Arrays.* Langmuir *26*, 1925-19229, **2010**.

[4] L.D. Landau, E. Lifshitz. *On the theory of the dispersion of magnetic permeability in ferromagnetic bodies.* Phys. Z. Sowjetunion *8*, 153-169, **1935**.

[5] J.D. Jackson in: *Classical Electrodynamics*, 2nd ed., Wiley, New York, **1975**.

[6] A. Weddemann, A. Auge, D. Kappe, F. Wittbracht, A. Hütten. *Dynamic simulations of the dipolar driven demagnetization process of magnetic multicore nanoparticles.* J. Magn. Magn. Mat. *322*, 643-646, **2010**.

[7] A. Weddemann, J. Jadidian, Y.S. Kim, S.R. Khushrushahi, M. Zahn. *Ferromagnetic materials for MEMS- and NEMS-devices.* Proc. COMSOL Conf., Boston, **2011**.

[8] A. Weddemann, C. Albon, A. Auge, F. Wittbracht, P. Hedwig, D. Akemeier, K. Rott, D. Meiner, P. Jutzi, A. Hütten. *How to design magneto-based total analysis systems for biomedical applications.* Biosens. Bioelec. *26*, 1152-1163, **2010**.

[9] P. Grünberg, R. Schreiber, Y. Pang, M.D. Brodsky, H. Sowers. *Layered Magnetic Structures: Evidence for Antiferromagnetic Coupling of Fe Layers across Cr Interlayers.* Phys. Rev. Lett. *57*, 2442-2445, **1986**.

[10] M.N. Baibich, J.M. Broto, A. Fert, F. Nguyen Van Dau, F. Petroff, P. Etienne, G. Creuzet, A. Friederich, J. Chazelas. *Giant Magnetoresistance of (001)Fe/(001)Cr Magnetic Superlattices.* Phys. Rev. Lett. *61*, 2472-2475, **1988**.

[11] A.E. Berkowitz, J.R. Mitchell, M.J. Carey, A.P. Young, S. Zhang, F.E. Spada, F.T. Parker, A. Hütten, G. Thomas. *Giant magnetoresistance in herterogeneous Cu-Co alloys.* Phys. Rev. Lett. *68*, 3745-3748, **1992**.

[12] J.Q. Xiao, S. Jiang, C.L. Chien. *Giant magnetoresistance in nonmultilayer magnetic systems.* Phys. Rev. Lett. *68*, 3749-3752, **1992**.

[13] N. Wiser. *Phenomenological theory of the giant magnetoresistance of superparamagnetic particles.* J. Magn. Magn. Mater. *159*, 119-124, **1996**.